Impact Factor:						
	ISRA (India)	= 6.317	SIS (USA)	= 0.912	ICV (Poland)	= 6.630
	ISI (Dubai, UAE)	= 1.582	РИНЦ (Russia)	= 3.939	PIF (India)	= 1.940
	GIF (Australia)	= 0.564	ESJI (KZ)	= 9.035	IBI (India)	= 4.260
	JIF	= 1.500	SJIF (Morocco)	= 7.184	OAJI (USA)	= 0.350

SOI: 1.1/TAS DOI: 10.15863/TAS
International Scientific Journal
Theoretical & Applied Science
p-ISSN: 2308-4944 (print) **e-ISSN:** 2409-0085 (online)
Year: 2021 **Issue:** 11 **Volume:** 103
Published: 18.11.2021 **http://T-Science.org**

QR – Issue QR – Article

Denis Chemezov
Vladimir Industrial College
M.Sc.Eng., Corresponding Member of International Academy of Theoretical and Applied Sciences, Lecturer, Russian Federation
https://orcid.org/0000-0002-2747-552X
vic-science@yandex.ru

Egor Prozorov
Vladimir Industrial College
Student, Russian Federation

Ivan Chebryakov
Vladimir Industrial College
Student, Russian Federation

Sergey Lukashov
Vladimir State University named after Alexander & Nikolay Stoletovs
Institute of Mechanical Engineering & Automobile Transport
Student, Russian Federation

Viktor Morozov
Vladimir Industrial College
Student, Russian Federation

Vladislav Samoylov
Vladimir Industrial College
Student, Russian Federation

Vyacheslav Matveev
Vladimir Industrial College
Student, Russian Federation

REFERENCE DATA OF PRESSURE DISTRIBUTION ON THE SURFACES OF AIRFOILS HAVING THE NAMES BEGINNING WITH THE LETTER A (THE SECOND PART)

Abstract: *The results of the computer calculation of air flow around the airfoils having the names beginning with the letter A are presented in the article. The contours of pressure distribution on the surfaces of the airfoils at the angles of attack of 0, 15 and -15 degrees in conditions of the subsonic airplane flight speed were obtained.*

Key words: *the airfoil, the angle of attack, pressure, the surface.*
Language: *English*
Citation: Chemezov, D., et al. (2021). Reference data of pressure distribution on the surfaces of airfoils having the names beginning with the letter A (the second part). *ISJ Theoretical & Applied Science, 11 (103),* 656-675.
Soi: http://s-o-i.org/1.1/TAS-11-103-64 ***Doi***: crossref https://dx.doi.org/10.15863/TAS.2021.11.103.64
Scopus ASCC: *1507.*

Introduction

Creating reference materials that determine the most accurate pressure distribution on the airfoils surfaces is an actual task of the airplane aerodynamics.

Materials and methods

The study of air flow around the airfoils was carried out in a two-dimensional formulation by means of the computer calculation in the *Comsol Multiphysics* program. The airfoils in the cross section were taken as objects of research [1-11]. In this work, the airfoils having the names beginning with the letter *A* (continuation [12]) were adopted. Air flow around the airfoils was carried out at the angles of attack (α) of 0, 15 and -15 degrees. The flight speed of the airplane in each case was subsonic. The airplane flight in the atmosphere was carried out under normal weather conditions. The geometric characteristics of the studied airfoils are presented in the Table 1. The studied geometric shapes of the airfoils in the cross section are presented in the Table 2.

Table 1. The geometric characteristics of the airfoils.

Airfoil name	Max. thickness	Max. camber	Leading edge radius	Trailing edge thickness
2032cjc	8.00% at 18.3% of the chord	7.00% at 35.0% of the chord	0.8668%	0.32%
Abrial 17-bis	9.89% at 20.0% of the chord	3.42% at 20.0% of the chord	0.4091%	0.1%
AG03	6.24% at 25.0% of the chord	2.02% at 32.7% of the chord	0.4353%	0.121%
AG04	6.42% at 22.5% of the chord	1.75% at 40.2% of the chord	0.4617%	0.134%
AG08	5.83% at 21.0% of the chord	1.8% at 39.1% of the chord	0.4494%	0.1599%
AG09	4.86% at 17.4% of the chord	1.86% at 32.8% of the chord	0.4879%	0.1953%
AG10	4.73% at 16.1% of the chord	1.71% at 32.6% of the chord	0.6852%	0.3617%
AG11	5.81% at 25.4% of the chord	2.29% at 29.1% of the chord	0.6035%	0.2321%
AG16	7.11% at 23.3% of the chord	1.87% at 46.9% of the chord	0.4682%	0.0929%
AG17	6.49% at 21.9% of the chord	2.02% at 45.5% of the chord	0.453%	0.0939%
AG18	5.87% at 20.6% of the chord	2.16% at 44.2% of the chord	0.4386%	0.0948%
AG19	5.4% at 20.6% of the chord	2.27% at 42.8% of the chord	0.4293%	0.0954%
AG24	8.41% at 26.0% of the chord	2.22% at 45.5% of the chord	0.5238%	0.0971%
AG25	7.58% at 24.6% of the chord	2.4% at 45.5% of the chord	0.4899%	0.0963%
AG26	6.84% at 23.3% of the chord	2.55% at 44.2% of the chord	0.4882%	0.0999%
AG27	6.11% at 21.7% of the chord	2.7% at 44.0% of the chord	0.4959%	0.1035%
AG12	6.24% at 21.9% of the chord	1.85% at 42.7% of the chord	0.4513%	0.0942%
AG13	5.83% at 21.0% of the chord	1.97% at 41.7% of the chord	0.4552%	0.0948%
AG14	5.37% at 19.9% of the chord	2.1% at 40.5% of the chord	0.452%	0.0956%
AG455ct – 02f rot.	6.47% at 23.3% of the chord	1.83% at 31.6% of the chord	0.5107%	0.0844%
AG45c – 03f	6.93% at 23.3% of the chord	2.58% at 38.7% of the chord	0.5214%	0.0893%
AG46c – 03f	6.03% at 23.3% of the chord	2.28% at 41.5% of the chord	0.4764%	0.0793%
AG46ct – 02f rot.	6.08% at 23.3% of the chord	1.69% at 33.0% of the chord	0.4866%	0.0793%
AG47c – 03f	5.06% at 22.0% of the chord	1.96% at 45.7% of the chord	0.4573%	0.0692%
AG47ct – 02f rot.	4.99% at 22.0% of the chord	1.3% at 33.1% of the chord	0.4658%	0.0693%
Anderson SPICA	11.72% at 30% of the chord	4.74% at 35.0% of the chord	1.2192%	0.0%
AS5045	15.0% at 37.4% of the chord	1.02% at 27.0% of the chord	1.1351%	0.25%
AS5046	16.0% at 37.2% of the chord	1.08% at 20.5% of the chord	1.4094%	0.268%
AS5048	17.98% at 40.6% of the chord	1.19% at 23.4% of the chord	1.7444%	0.299%
ASW22 7.33m de MCM	17.45% at 31.4% of the chord	3.51% at 37.8% of the chord	2.9919%	0.2602%
ASW-7.33m de MCM	12.97% at 27.0% of the chord	3.51% at 37.6% of the chord	1.721%	0.193%
AVISTAR	14.52% at 34.2% of the chord	2.19% at 37.9% of the chord	2.3196%	0.3211%

Note:
AG03, AG11 (Apogee HLG series wood wing Mark Drela);
AG04-AG10 (Apogee HLG series molded wing composite Mark Drela);
AG16-AG19 (Allegro 2m 1 Mark Drela);
AG24-AG27 (Bubble Dancer DLG by Mark Drela);
AG12-AG14 (New SuperGee DLG by Mark Drela);
AG455ct – 02f rot., AG46ct – 02f rot., AG47ct – 02f rot. (New SuperGee DLG by Mark Drela);
AG45c – 03f, AG46c – 03f, AG47c – 03f (SuperGee RC DLG by Mark Drela);
Anderson SPICA (R/C sailplane airfoil, smoothed);
AS5045 (Ashok Gopalarathnam/Selig 15% at the tip), *AS5046* (Ashok Gopalarathnam/Selig 16% will work on stock spars), *AS5048* (Ashok Gopalarathnam/Selig 18% at the root);
AVISTAR (Hobbico R/C Avistar trainer airfoil).

Table 2. The geometric shapes of the airfoils in the cross section.

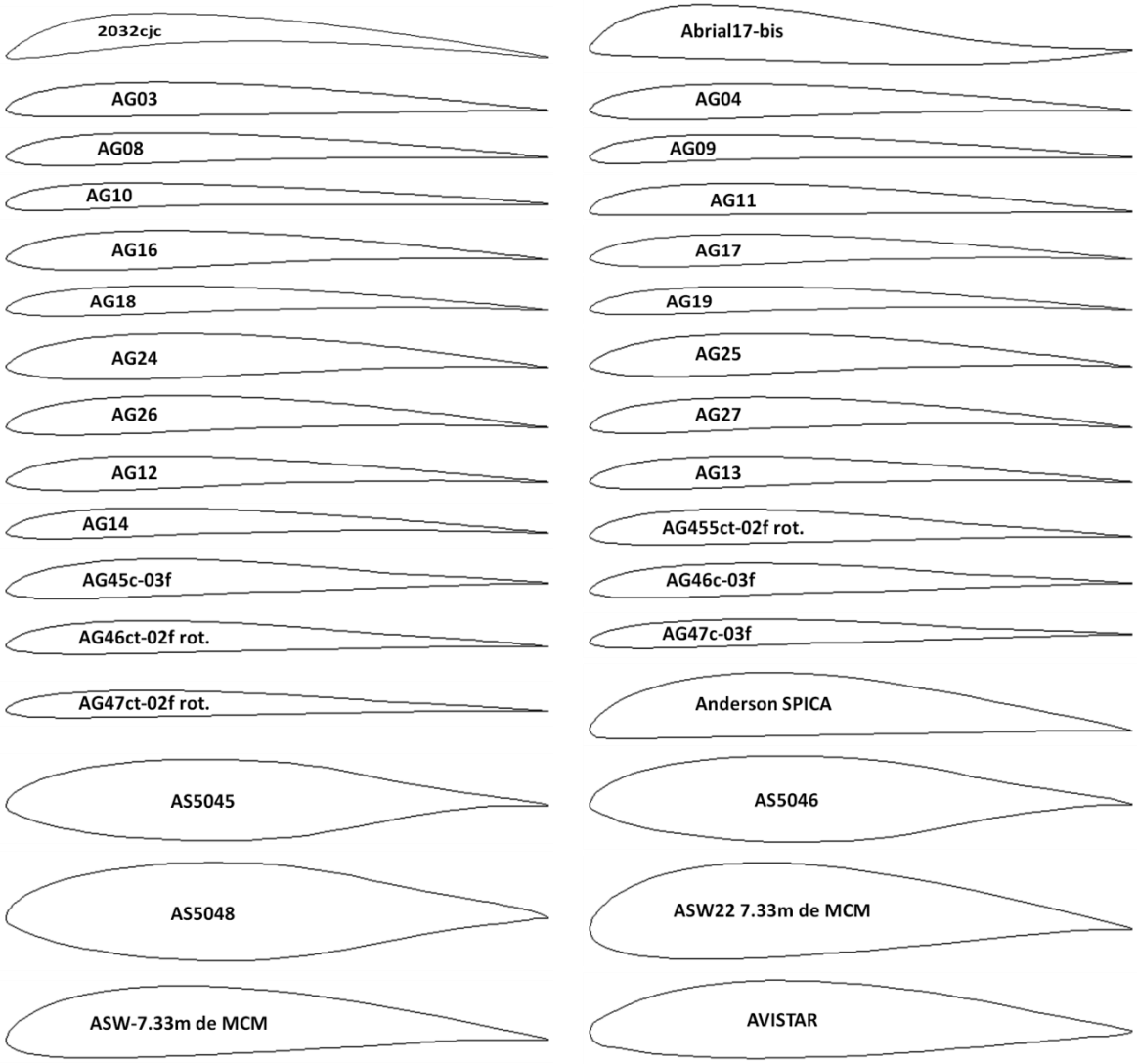

Results and discussion

The calculated pressure contours on the surfaces of the airfoils at the different angles of attack are presented in the Figs. 1-32. The calculated magnitudes on the scale can be represented as the basic magnitudes when comparing the pressure drop under conditions of changing the angle of attack of the airfoils.

When comparing the 20-32C and 2032cjc airfoils, it was determined that at the zero angle of attack, the calculated pressure magnitudes on the surfaces are the same. The calculated pressure magnitudes increase at the positive and negative angles of attack. The Abrial 17-bis airfoil undergoes less deformations in the horizontal position than the Abrial 17 airfoil. However, at the positive and negative angles of attack, the Abrial 17-bis modified airfoil is subjected to more pressure than the original version.

The occurrence of the negative pressure gradient over the larger area of the upper surface at the zero angle of attack is characteristic of the AG airfoils line. Drag increases at the leading edge from the side of the upper surface of the airfoil at the positive and negative angles of attack. Pressure is distributed evenly over the areas of the upper and lower surfaces. Maximum pressure of -91.7 kPa is determined at the angle of attack of 15 degrees of the AG03 airfoil, minimum pressure of -1.93 kPa is determined at the angle of attack of 0 degrees of the AG47c – 03f airfoil.

The airfoils with the maximum thickness are characterized by the formation of the negative pressure gradient over the large areas of the upper and lower surfaces at the positive and negative angles of attack. Acting pressure decreases with increasing the airfoil thickness (for example, AS5045, AS5046, AS5048).

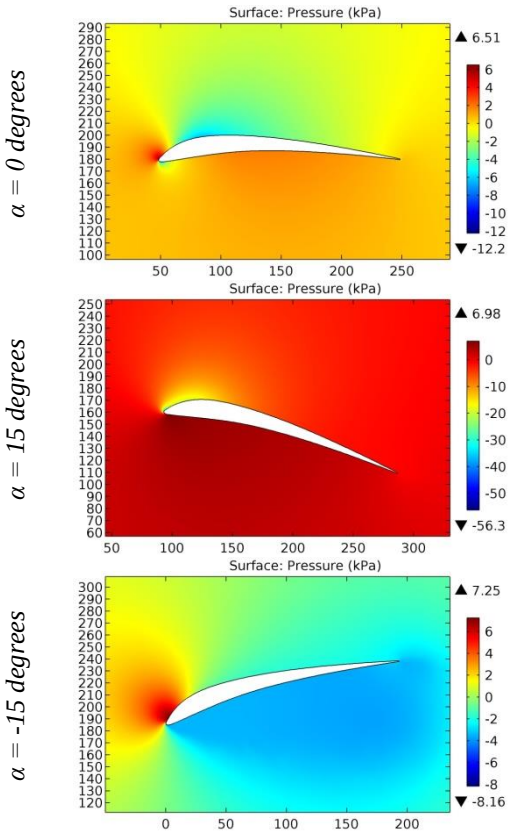

Figure 1. The pressure contours on the surfaces of the 2032cjc airfoil.

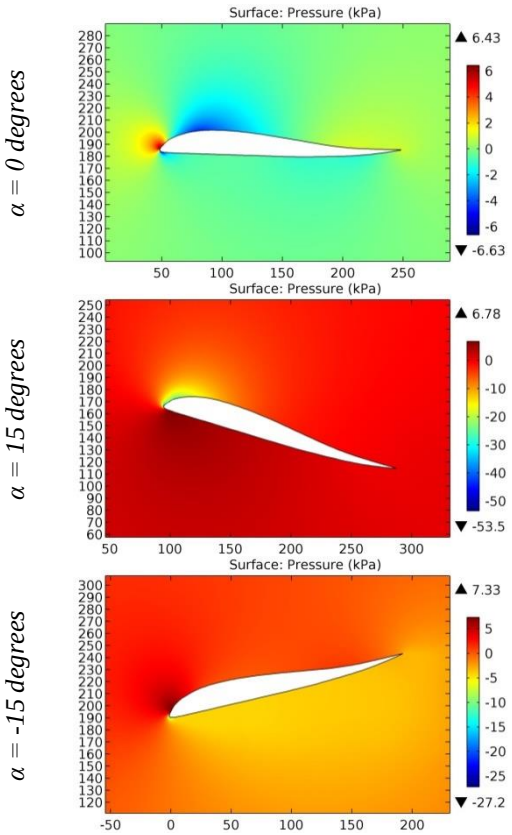

Figure 2. The pressure contours on the surfaces of the Abrial 17-bis airfoil.

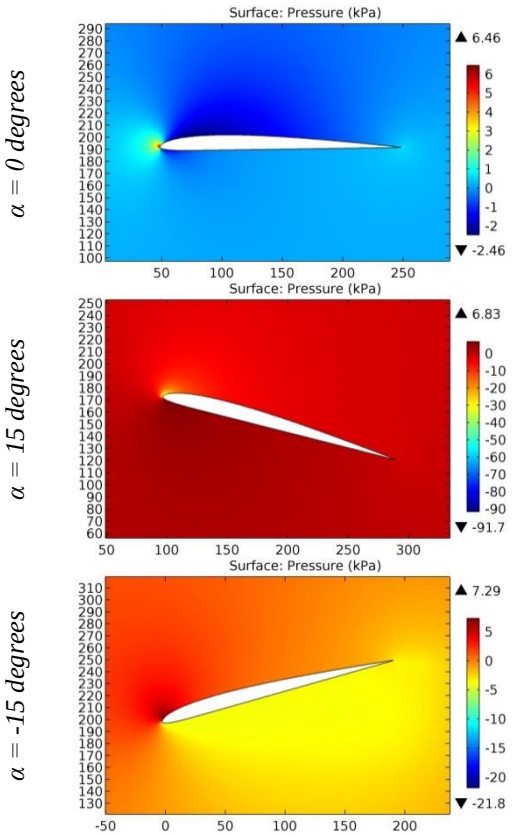

Figure 3. The pressure contours on the surfaces of the AG03 airfoil.

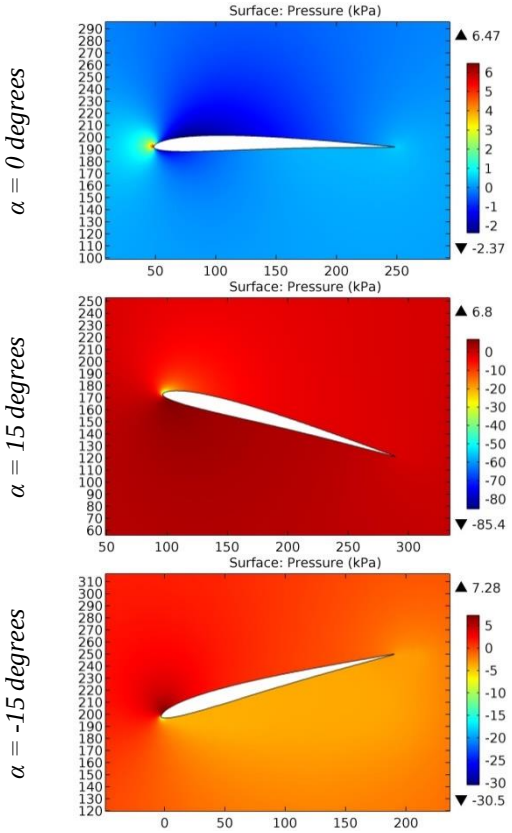

Figure 4. The pressure contours on the surfaces of the AG04 airfoil.

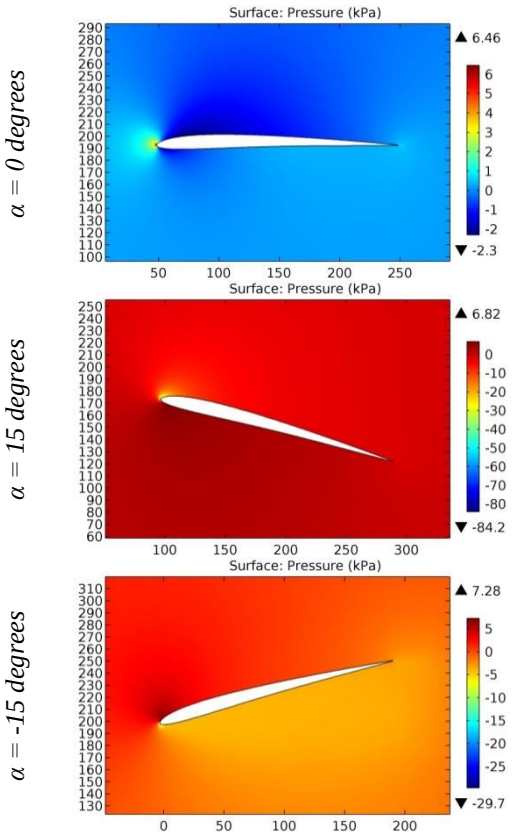

Figure 5. The pressure contours on the surfaces of the AG08 airfoil.

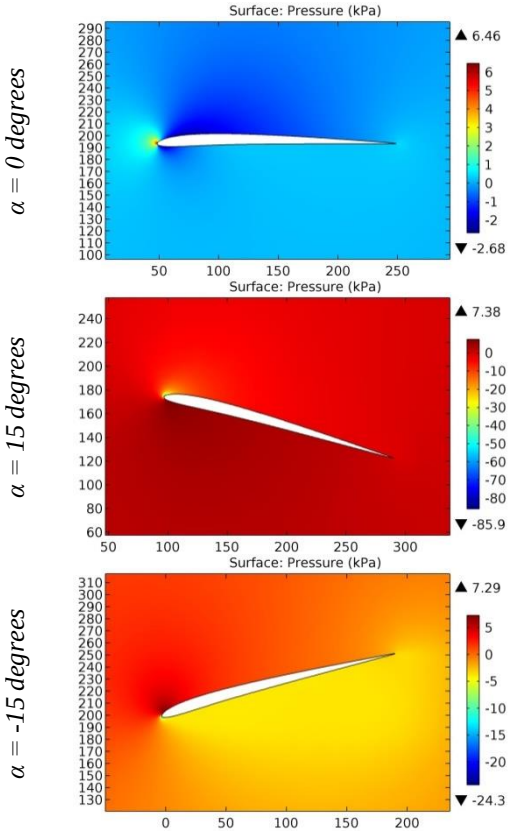

Figure 6. The pressure contours on the surfaces of the AG09 airfoil.

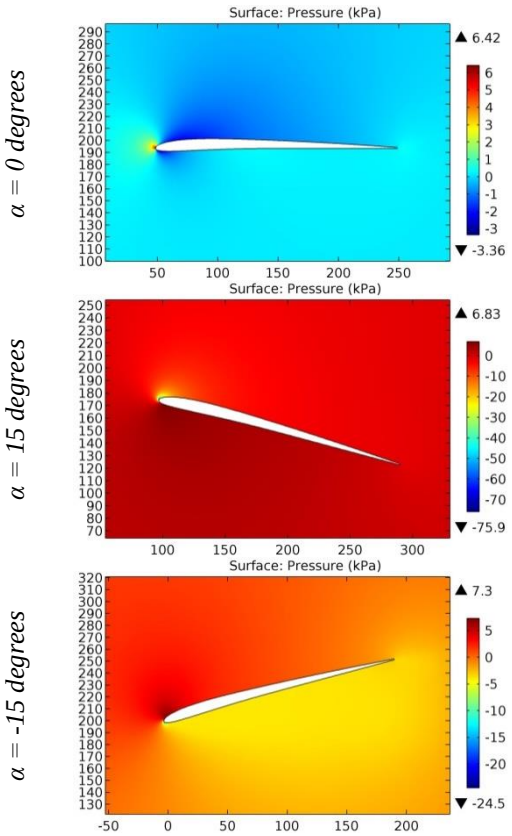

Figure 7. The pressure contours on the surfaces of the AG10 airfoil.

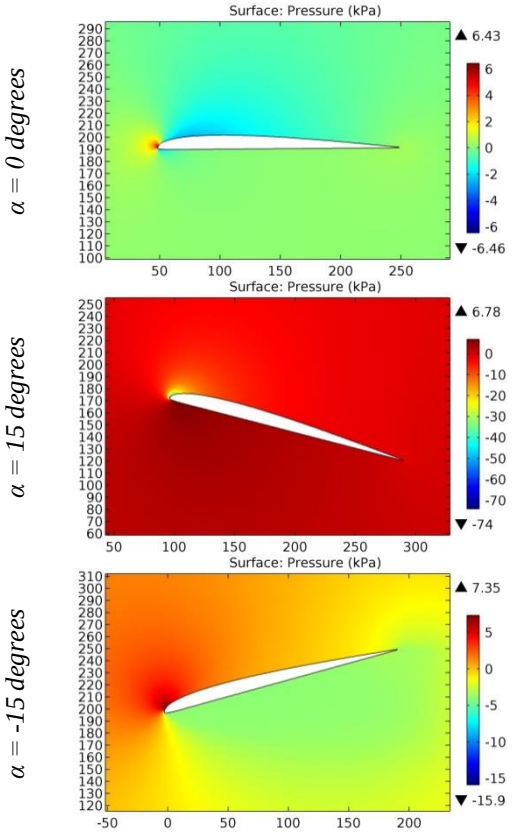

Figure 8. The pressure contours on the surfaces of the AG11 airfoil.

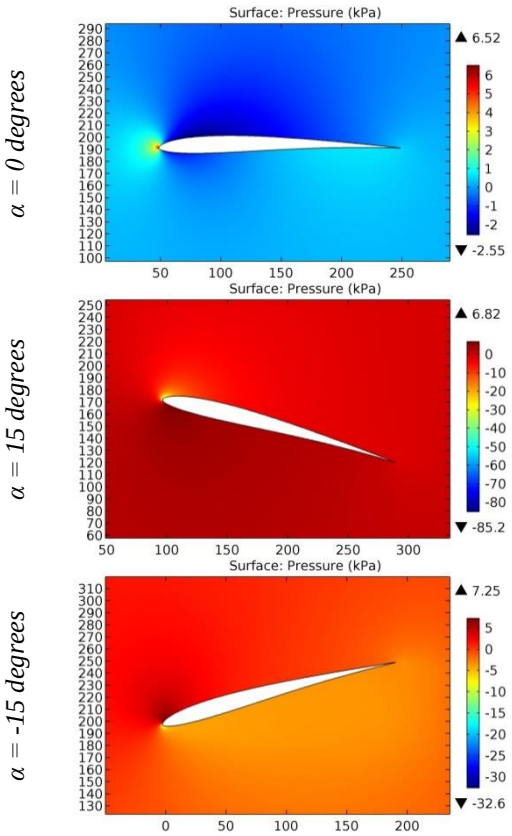

Figure 9. The pressure contours on the surfaces of the AG16 airfoil.

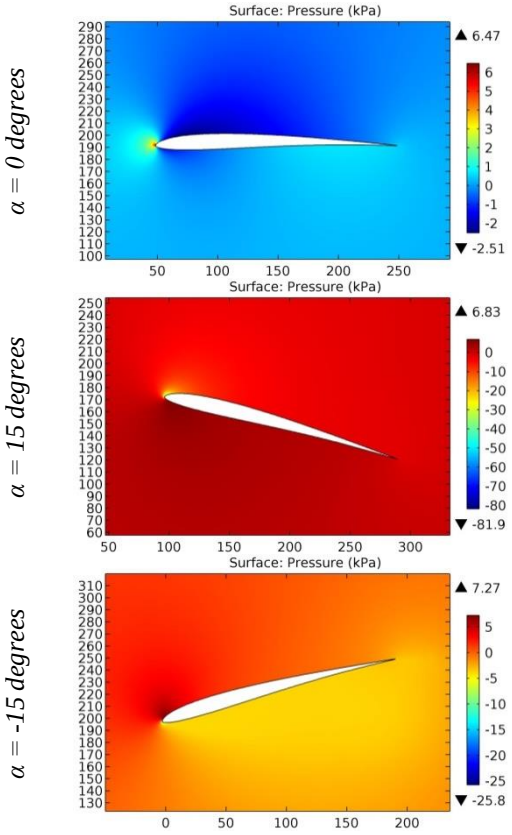

Figure 10. The pressure contours on the surfaces of the AG17 airfoil.

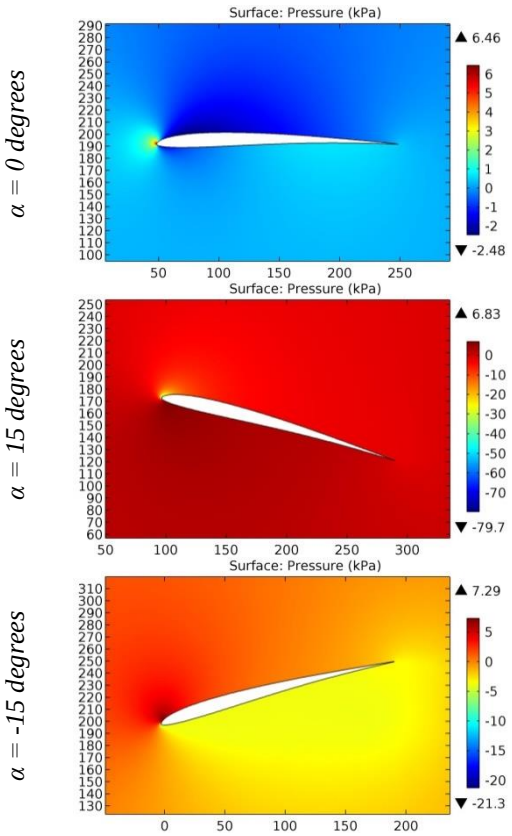

Figure 11. The pressure contours on the surfaces of the AG18 airfoil.

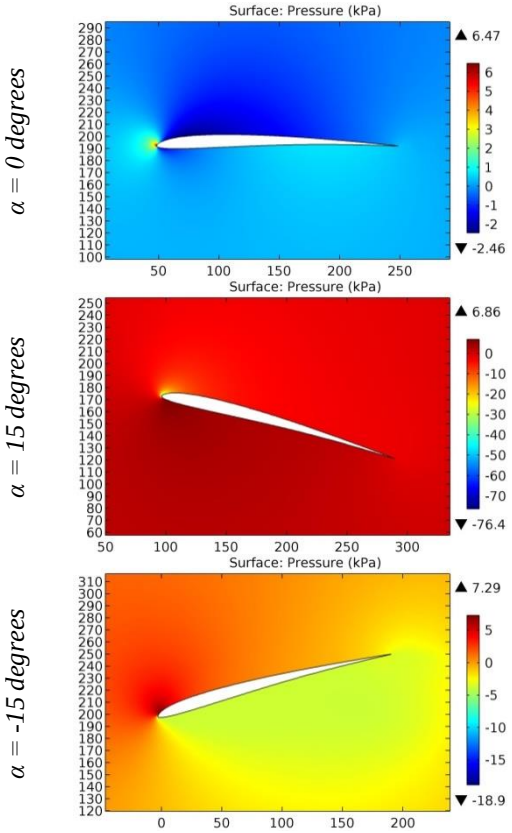

Figure 12. The pressure contours on the surfaces of the AG19 airfoil.

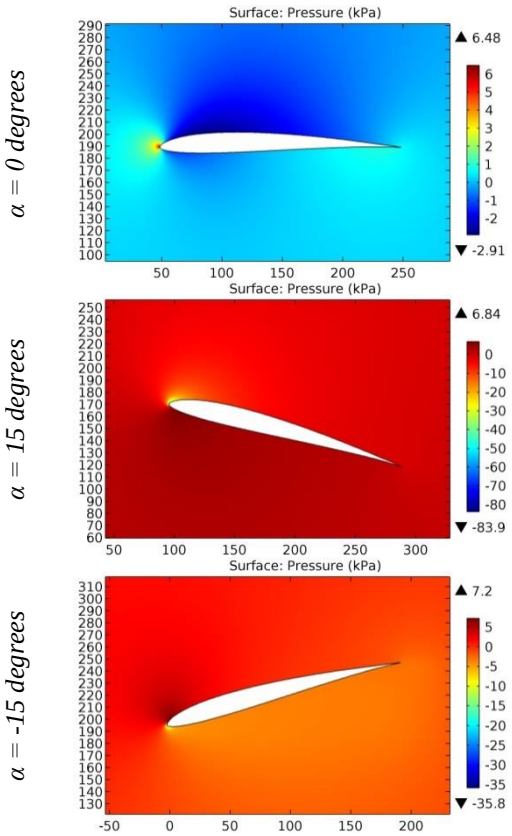

Figure 13. The pressure contours on the surfaces of the AG24 airfoil.

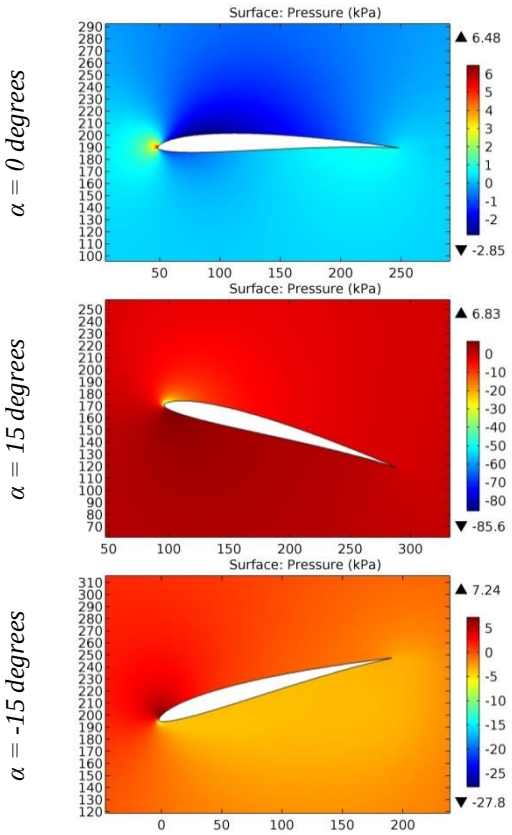

Figure 14. The pressure contours on the surfaces of the AG25 airfoil.

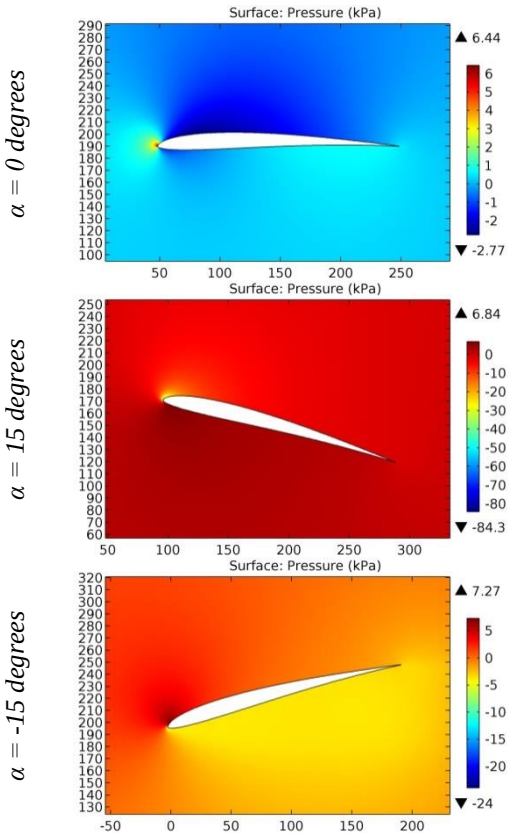

Figure 15. The pressure contours on the surfaces of the AG26 airfoil.

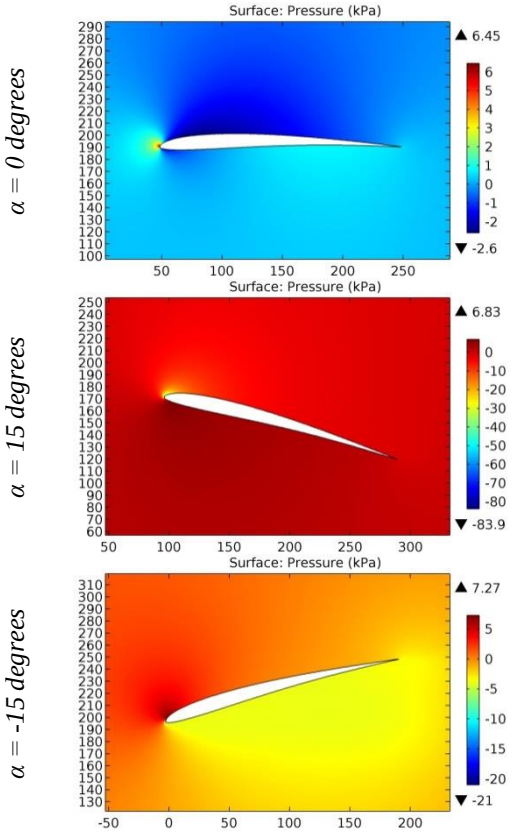

Figure 16. The pressure contours on the surfaces of the AG27 airfoil.

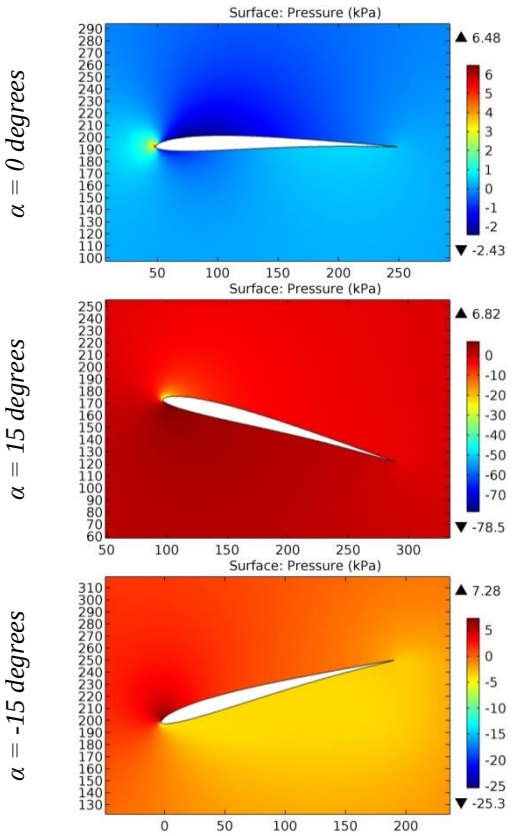

Figure 17. The pressure contours on the surfaces of the AG12 airfoil.

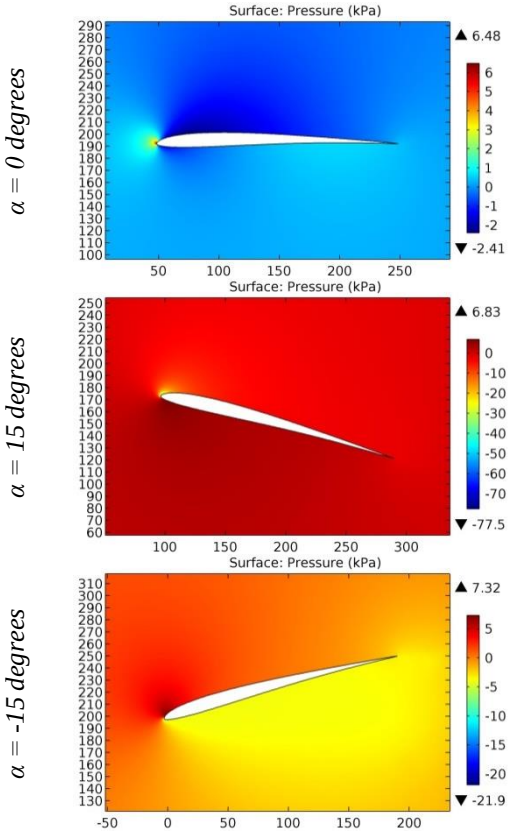

Figure 18. The pressure contours on the surfaces of the AG13 airfoil.

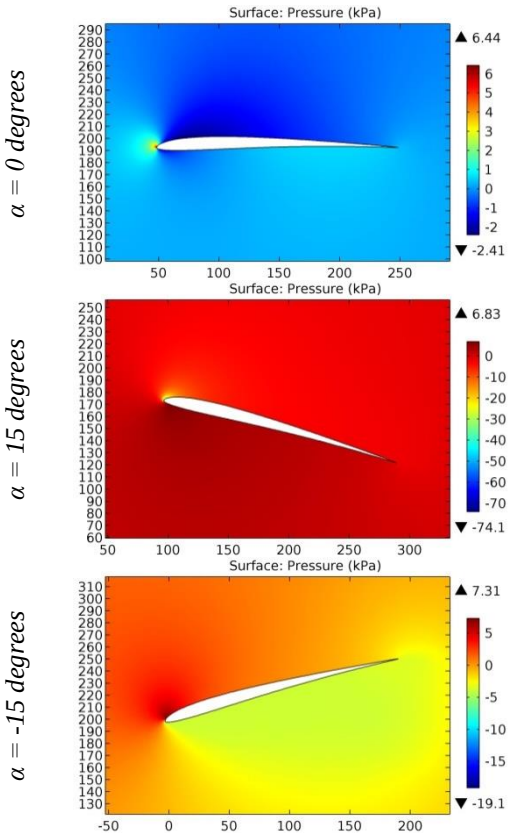

Figure 19. The pressure contours on the surfaces of the AG14 airfoil.

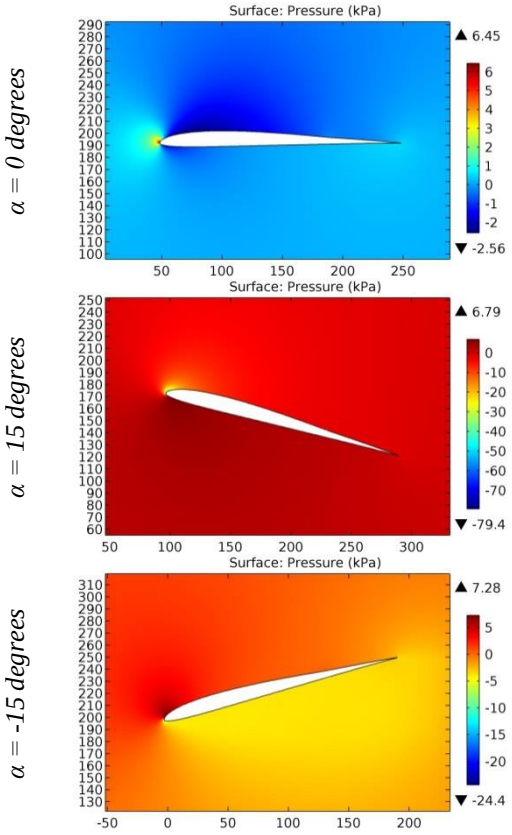

Figure 20. The pressure contours on the surfaces of the AG455ct – 02f rot airfoil.

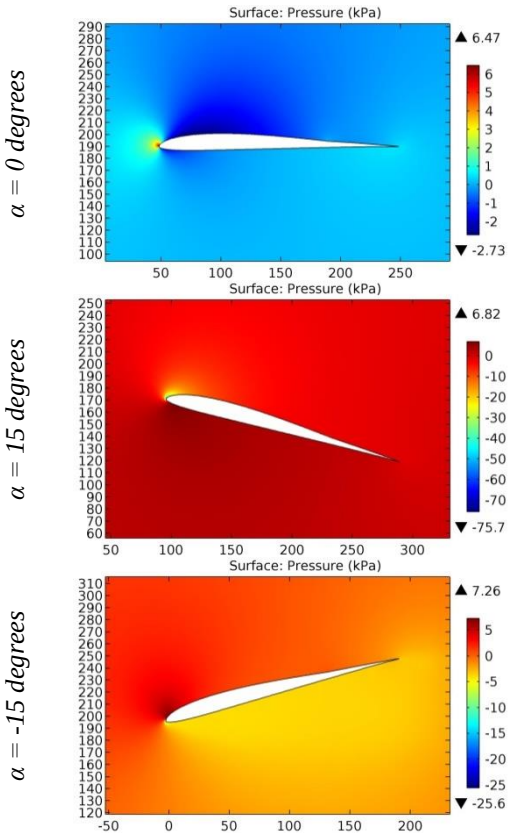

Figure 21. The pressure contours on the surfaces of the AG45c – 03f airfoil.

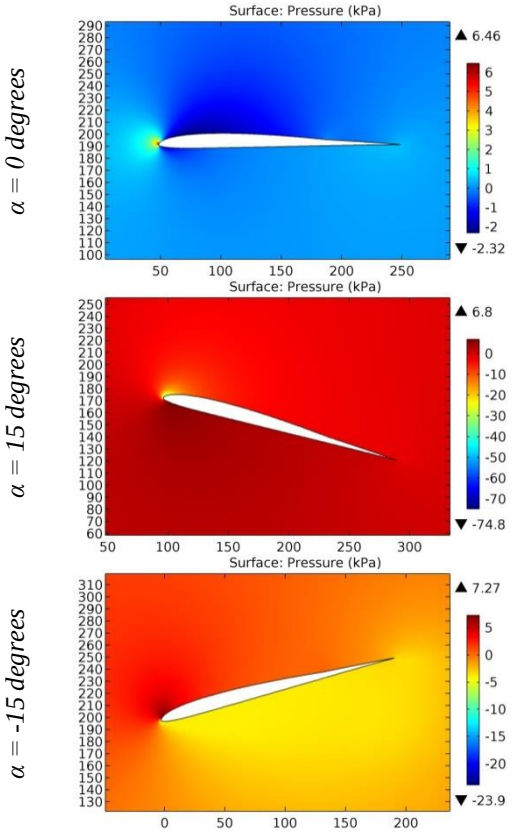

Figure 22. The pressure contours on the surfaces of the AG46c – 03f airfoil.

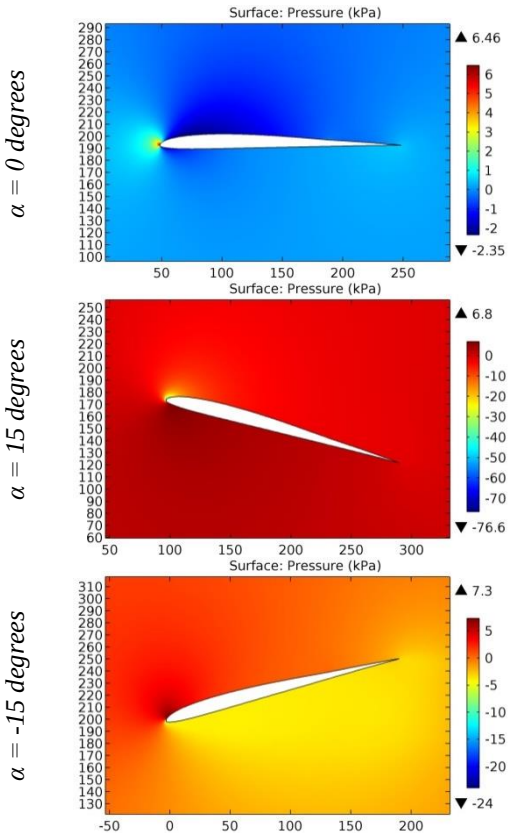

Figure 23. The pressure contours on the surfaces of the AG46ct – 02f rot airfoil.

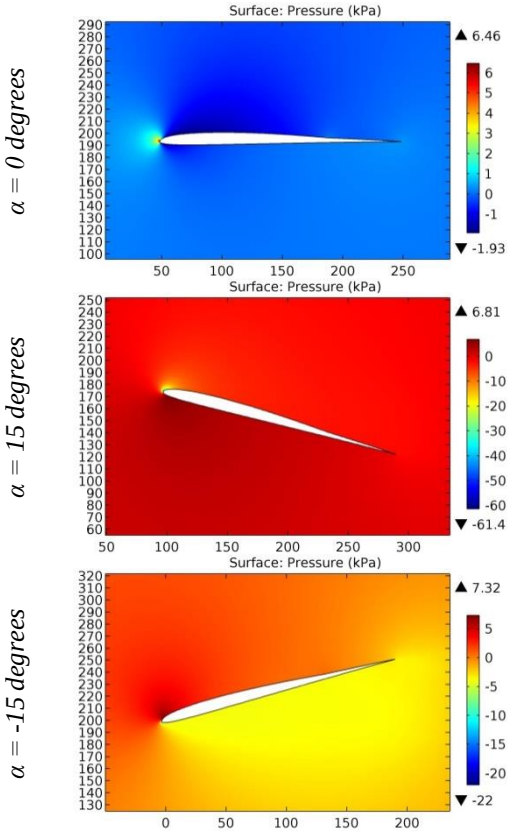

Figure 24. The pressure contours on the surfaces of the AG47c – 03f airfoil.

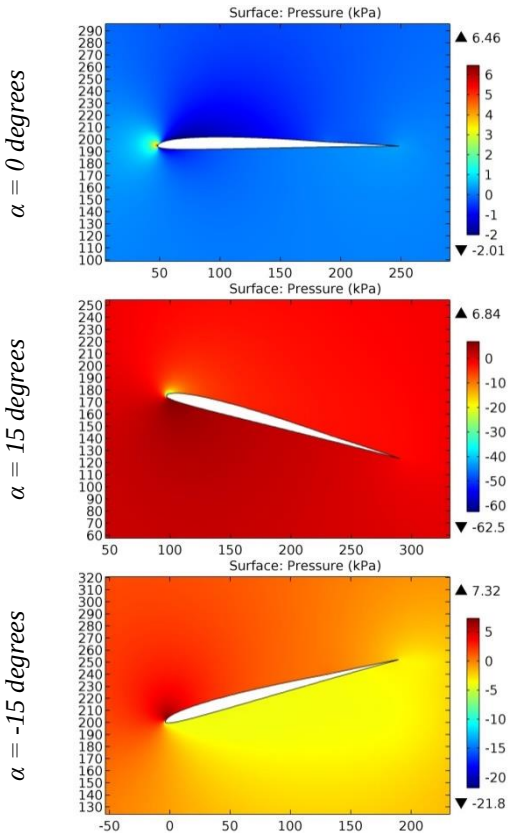

Figure 25. The pressure contours on the surfaces of the AG47ct – 02f rot airfoil.

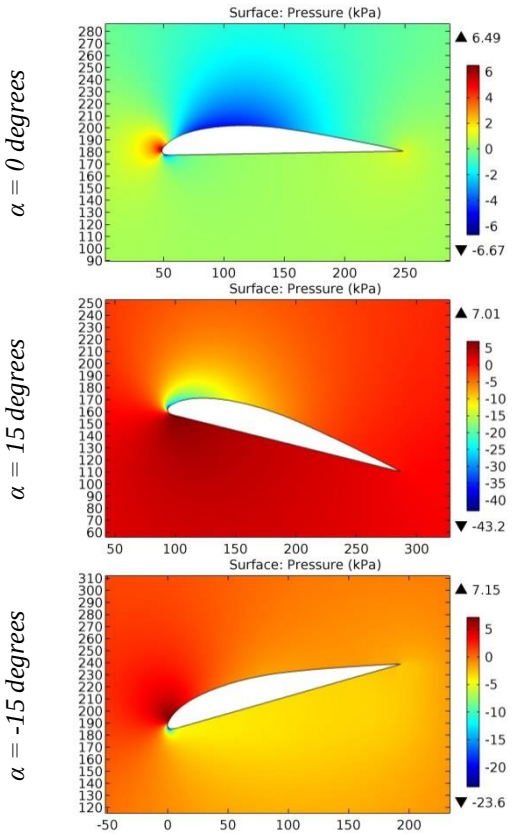

Figure 26. The pressure contours on the surfaces of the Anderson SPICA airfoil.

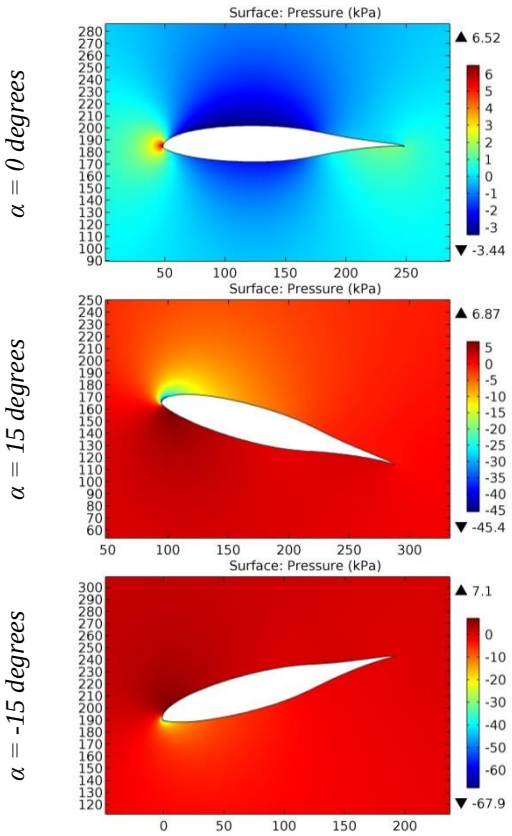

Figure 27. The pressure contours on the surfaces of the AS5045 airfoil.

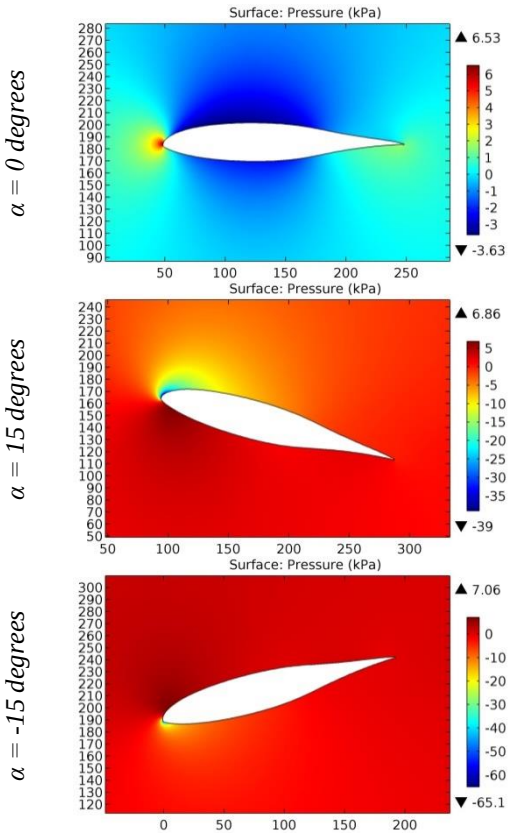

Figure 28. The pressure contours on the surfaces of the AS5046 airfoil.

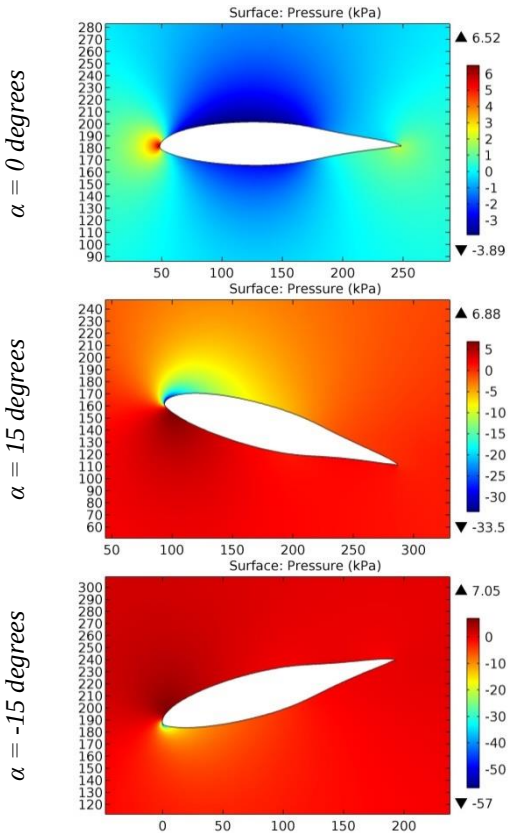

Figure 29. The pressure contours on the surfaces of the AS5048 airfoil.

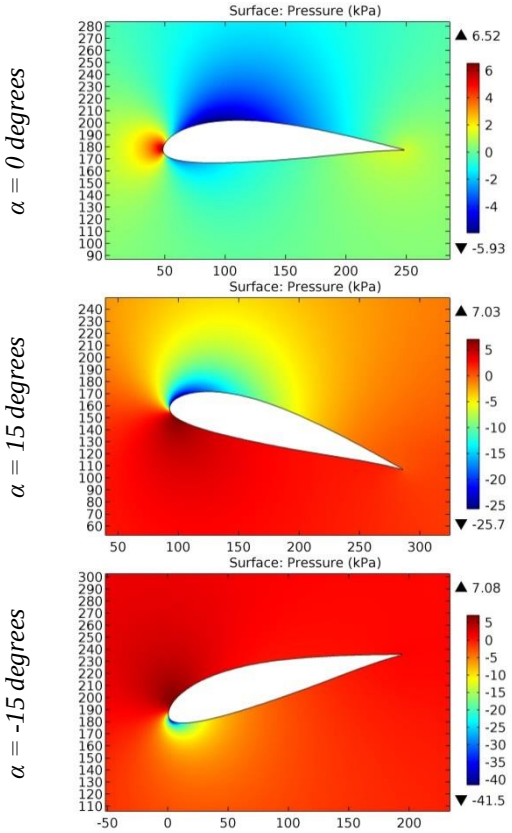

Figure 30. The pressure contours on the surfaces of the ASW22 7.33m de MCM airfoil.

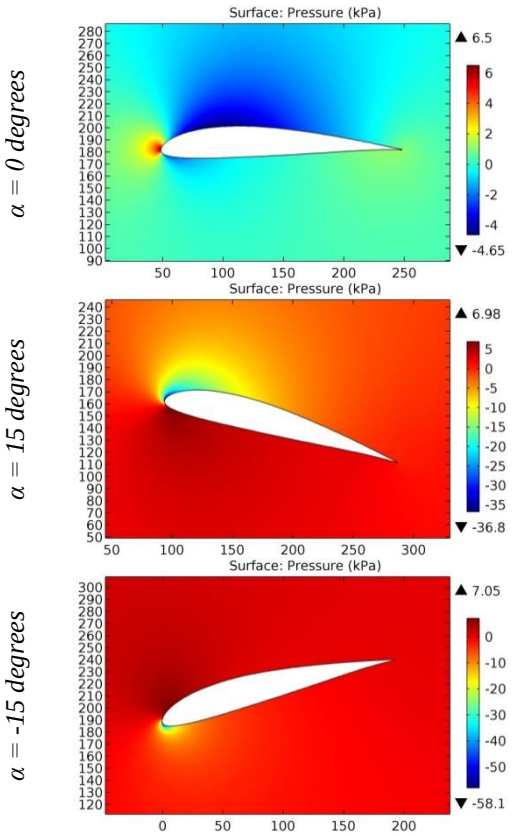

Figure 31. The pressure contours on the surfaces of the ASW-7.33m de MCM airfoil.

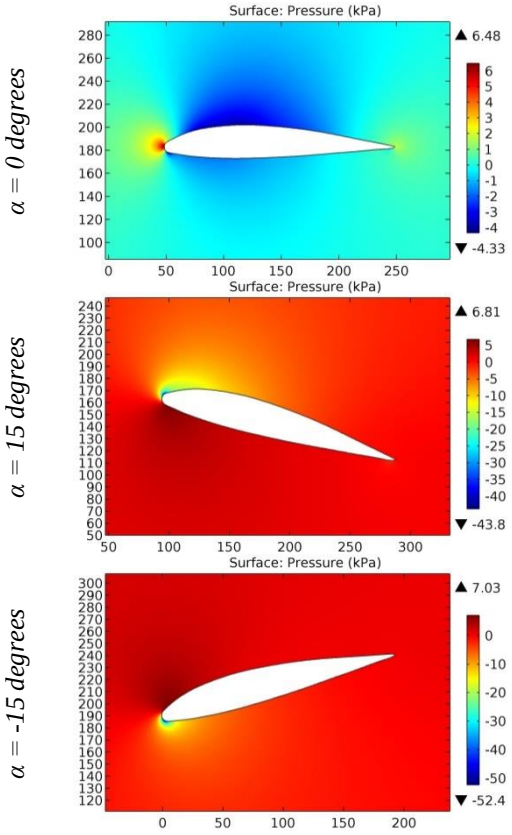

Figure 32. The pressure contours on the surfaces of the AVISTAR airfoil.

For the some airfoils, maximum increase in negative pressure on the leading edge occurs at the angle of attack of 15 degrees (2032cjc, Abrial 17-bis, AG03-AG27, AG455ct – 02f rot., AG45c – 03f, AG46c – 03f, AG46ct – 02f rot., AG47c – 03f, AG47ct – 02f rot., Anderson SPICA), and for others, increase in negative pressure on the leading edge occurs at the angle of attack of -15 degrees (AS5045, AS5046, AS5048, ASW22 7.33m de MCM, ASW-7.33m de MCM, AVISTAR).

Conclusion

The considered airfoils with the maximum thickness are characterized by an increase in drag at the leading edge in conditions of maneuvering the airplane, leading to a decrease in the flight altitude. Drag increases several times during takeoff of the airplane for the rest airfoils. Maximum pressure is negative and for two airfoils (AG03 and AG09) it is -91.7 kPa and -85.9 kPa, respectively.

References:

1. Anderson, J. D. (2010). Fundamentals of Aerodynamics. *McGraw-Hill, Fifth edition*.
2. Shevell, R. S. (1989). Fundamentals of Flight. *Prentice Hall, Second edition.*
3. Houghton, E. L., & Carpenter, P. W. (2003). Aerodynamics for Engineering Students. *Fifth edition, Elsevier*.
4. Lan, E. C. T., & Roskam, J. (2003). Airplane Aerodynamics and Performance. *DAR Corp*.
5. Sadraey, M. (2009). Aircraft Performance Analysis. *VDM Verlag Dr. Müller*.
6. Anderson, J. D. (1999). Aircraft Performance and Design. *McGraw-Hill*.
7. Roskam, J. (2007). Airplane Flight Dynamics and Automatic Flight Control, Part I. *DAR Corp*.
8. Etkin, B., & Reid, L. D. (1996). Dynamics of Flight, Stability and Control. *Third Edition, Wiley*.
9. Stevens, B. L., & Lewis, F. L. (2003). Aircraft Control and Simulation. *Second Edition, Wiley*.
10. Chemezov, D., et al. (2021). Pressure distribution on the surfaces of the NACA 0012 airfoil under conditions of changing the angle of attack. *ISJ Theoretical & Applied Science, 09 (101)*, 601-606.
11. Chemezov, D., et al. (2021). Stressed state of surfaces of the NACA 0012 airfoil at high angles of attack. *ISJ Theoretical & Applied Science, 10 (102)*, 601-604.
12. Chemezov, D., et al. (2021). Reference data of pressure distribution on the surfaces of airfoils having the names beginning with the letter A (the first part). *ISJ Theoretical & Applied Science, 10 (102)*, 943-958.